Characterization of Nonideal Networks by Stress–Strain Measurements at Large Extensions

M. KLÜPPEL

Deutsches Institut für Kautschuktechnologie e. V., Eupener Straße 33, 3000 Hannover 81, Germany

SYNOPSIS

It is shown how a characterization of unfilled, amorphous rubber networks can be evaluated from uniaxial stress–strain measurement data. Beside the cross-linking density, the relative scission probability during the curing procedure is evaluated, which determines the amount of dangling free chain ends and the number of trapped entanglements. These values are found from the C_2 term of the Mooney–Rivlin equation by using the predictions of a tube model. A necessary requirement for applying stress–strain measurements at large extensions is the consideration of the finite extensibility component of the reduced stress. It is taken into account by using a numerical procedure, which derives from a series expansion of the inverse Langevin approximation. The experimental results found at natural rubber networks cross-linked with thiuram (TMTD) and peroxid (DCP) show that network defects cannot be neglected in the DCP networks. They are assumed to be connected to the worse tensil strength properties compared to the TMTD networks. © 1993 John Wiley & Sons, Inc.

1. INTRODUCTION

The physics of rubber elasticity is characterized by a great variety of approaches, models, and concepts. This has been reviewed in a considerable number of papers.[1-7] The first remarkable molecular interpretation of rubber elasticity was introduced by Kuhn, Guth, and Mark.[8,9] They developed the statistical mechanics of polymer chains by describing the configuration and conformation of the monomeric units in a random flight model of statistical segments. This is the basic assumption of the so-called Gaussian chain model, where the end-to-end distance of the chains results in a Gaussian distribution function. The elastic forces are calculated from the conformational entropy loss of the network chains, when the mean end-to-end distance deviates from its most probable value.

Based on this general concept, different approaches to the description of the real stress–strain behavior of amorphous polymer networks have been developed. Essentially, additional assumptions concerning the influence of the surrounding chains on the entropy of a single network chain were made. Flory and Erman[10-13] and, independently, Kästner[14-17] developed a concept of restricted junction fluctuations, while the network chains themselves were handled as phantom chains, which do not feel any constraints. By assuming the free fluctuation space of the cross-linking junctions to be transformed nonaffinely under deformation, this model predicts nonaffine transformation properties on small length scales. This result is confirmed by NMR measurements of Gronski et al.[18] The deformation dependency of the reduced stress, as characterized by the phenomenological Mooney–Rivlin equation, is explained by a constraint release effect. In the infinite-strain limit, the restrictions on junction fluctuations disappear asymptotically and a pure phantom network results.

A more realistic approach to the consideration of topological constraints in real polymer networks are the tube models or related models like the slip-link model (compare Fig. 1). The most fundamental conception in this area was developed by Heinrich et al.,[19-23] who calculated the constraining tube diameter and its deformation dependency for a single-chain self-consistently from the free energy of the surrounding chains. This model works without any

Journal of Applied Polymer Science, Vol. 48, 1137–1150 (1993)
 CCC 0021-8995/93/071137-14

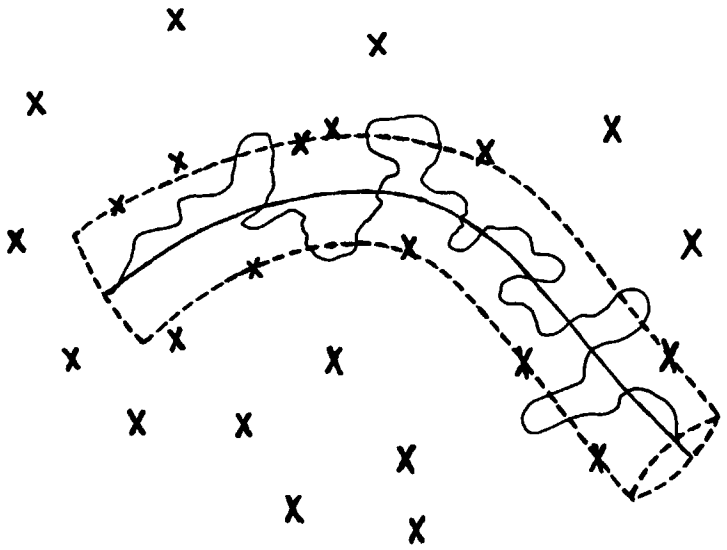

Figure 1 Schematic representation of a network chain in a tube. The tube diameter is given by the mean spacing of the topological constraint centers, i.e., cross-links and entanglements, indicated as crosses.

fitting parameters and explains the stress–strain data of uniaxial as well as biaxial extension in terms of molecular quantities. For highly cross-linked networks, their model leads to the semiempirical relation of Tschoegl,[24] which was found by comparing stress-relaxation experiments of cross-linked and uncross-linked materials. In the infinite-strain limit, the influence of the surrounding chains on the retracting force of a single chain releases asymptotically. This prediction compares to the one that is found in the model of restricted junction fluctuations. However, the tube model does not necessarily predict a free fluctuating phantom network in the infinite-strain limit. This is an essential difference between the two models.

So far, all problems concerning the elasticity of amorphous polymer networks seem to be solved. However, measurements of the microscopic properties by NMR spectroscopy are not in full agreement with the theoretical predictions. Especially, the calculated chemical cross-linking densities as found from the C_1 term of the Mooney–Rivlin equation in some cases clearly differ from those found from NMR measurements.[25] A possible explanation of this discrepancy is a wrong interpretation of the infinite-strain modulus, i.e., the C_1 term of the Mooney–Rivlin equation. It is generally believed that this modulus reflects the pure chemical cross-links, but this attempt of explanation contradicts the assumption that permanently trapped entanglements exist in polymer networks that behave somehow like chemical junctions. A detailed model for the behavior of trapped entanglements is presented in Ref. 7 or Ref. 26, but, in agreement with the usual interpretation, this model predicts a disappearing influence of the trapped entanglements on the infinite-strain modulus. A contribution to the equilibrium modulus is supposed only for small deformation.

This result is not easy to understand because trapped entanglements are not temporary and, thus, should contribute to every equilibrium modulus. Even in the case of minimal action, where all trapped entanglements slide onto a chemical netpoint, a nonzero efficiency of the trapped entanglements is expected, which results from the rise of the functionality of these netpoints. Instead, the experimental results seem to indicate that this picture does not work, because the infinite-strain modulus seems to change in direct proportionality with the amount of cross-linking agent. However, we will show below that this is not the case if non-Gaussian chain statistics are applied. We will find clear evidence for an influence of the trapped entanglements on the infinite-strain modulus, which means that the calculated chemical cross-linking densities are generally smaller than in the Gaussian case.

2. NON-GAUSSIAN CHAIN STATISTICS AND THE TUBE MODEL

Instead of the Gaussian distribution function for the end-to-end distance of a network chain, we assume the more realistic inverse Langevin approximation,

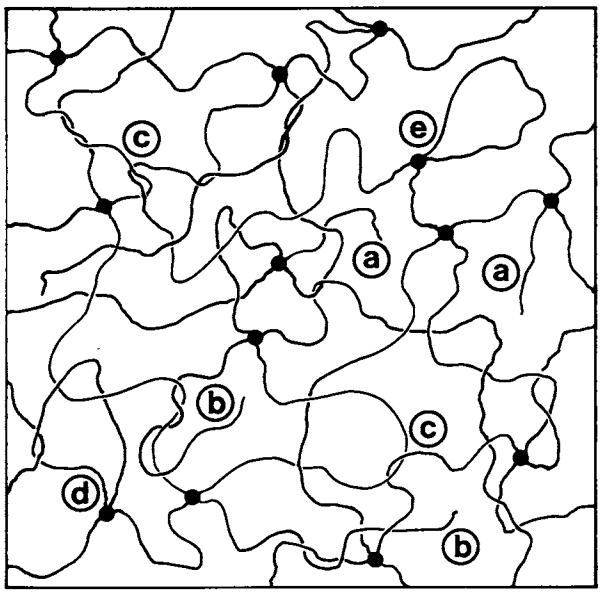

Figure 2 Schematic representation of a nonideal network: (a, b) dangling free chain ends; (b) with temporary entanglements; (c) trapped entanglements; (d, e) elastically effective and ineffective close loops, respectively.

introduced by Kuhn and Grün.[27] This approach takes into account the finite extensibility of the chains by considering the orientation of the statistical segments in the direction of strain. Thus, it can be applied up to large extensions, where the end-to-end distance approaches the fully extended length of the network chains. A very useful series expansion for the inverse Langevin function was used by Kuhn and Kuhn.[28] For uniaxial deformations, it leads to the following series expansion of the reduced stress (see, e.g., Ref. 1):

$$\sigma_{red} = G(\lambda)\left\{1 + \frac{3}{25n}\left(3\lambda^2 + \frac{4}{\lambda}\right) + \frac{297}{6125n^2}\left(5\lambda^4 + 8\lambda + \frac{8}{\lambda^2}\right) + \frac{12312}{2205000n^3}\left(35\lambda^6 + 60\lambda^3 + 72 + \frac{64}{\lambda^3}\right) + \frac{126117}{693673750n^4}\left(630\lambda^8 + 1120\lambda^5 + 1440\lambda^2 + \frac{1536}{\lambda} + \frac{1280}{\lambda^4}\right) + \cdots\right\} \quad (1)$$

with

$$\sigma_{red} = \frac{\sigma}{\lambda - \lambda^{-2}} \quad (2)$$

λ is the deformation ratio and σ is the stress related to the cross section of the undeformed sample; n is the average number of statistical segments of the network strands. For $\lambda = \sqrt{n}$, the full series expansion (1) approaches infinity. Thus, the square root of n defines the maximum deformation ratio of the network chains. In the limit $n \to \infty$, a Gaussian statistic results, i.e., the modulus $G(\lambda)$ is the Gaussian contribution to the reduced stress. This Gaussian modulus is, in general, unknown, as long as n is unknown. However, in the framework of the above-described molecular models on rubber elasticity, n can be determined as a function of $G(\lambda)$. By inserting this function into (1), n can be calculated and the finite extensibility component can be separated from the Gaussian contribution of the reduced stress. We will demonstrate how this works for the tube model.

2.1. A Numerical Procedure for Separating the Finite Extensibility Component of the Reduced Stress

Following the conception of the topological constraints in dry rubber networks as formulated in the tube model, we assume a two-network model with an elastic contribution G_1 and a topological constraint part $G_2 \cdot \phi(\lambda)$ that approaches zero in the infinite-strain limit $\lambda \to \infty$:

$$G(\lambda) = G_1 + G_2 \cdot \phi(\lambda) \approx G_1 + G_2 \frac{1}{\lambda} \quad \text{for } \lambda \geq 1;\ 0 < \beta \leq 1\ ^* \quad (3)$$

with

$$\phi(\lambda) = \frac{2(\lambda^{\beta/2} - \lambda^{-\beta})}{\beta(\lambda^2 - \lambda^{-1})} \quad (4)$$

β is a tube relaxation parameter, which is taken to be one in dry rubber networks, while in highly swollen networks, it equals zero. By applying elementary network theory, we assume

$$G(\lambda) = A\nu(\lambda)RT \quad (5)$$

R is the gas law constant; T, the absolute temperature; and A, a structure factor that depends on the

* For $\lambda \geq 1$, the function $\phi(\lambda)$ is well approximated by λ^{-1}, which corresponds to the semiempirical Mooney–Rivlin equation. However, this is not correct for $\lambda < 1$. In this case, only $\phi(\lambda)$ gives a good fit to experimental results.

amount of fluctuations of the cross-links. In a first approximation, we assume a structure factor of free fluctuating cross-links: $A = 1\text{–}2/f$, where f is the functionality of the cross-links. $\nu(\lambda)$ is a formal strand density that is constructed from the elastic as well as the constraining contribution†:

$$\nu(\lambda) = \nu_1 + \nu_2\phi(\lambda) \tag{6}$$

The strain-dependent strand density $\nu_2\phi(\lambda)$ corresponds to a pseudonetwork that describes the influence of the constraining tubes on the modulus. In this sense, it also reflects the influence of the constraining tubes on the degree of orientation of the statistical chain segments. This orientation is taken into consideration in the inverse Langevin approximation (1) by the strain λ and by the mean number of statistical segments n, which becomes strain-dependent in this model if it is coupled to the elastically effective strand density $\nu(\lambda)$. This means that the quantity $n(\lambda)$ is only a formal mean number of statistical segments, which is derived by considering all elastically effective strands: the real ones as well as those of the constraining pseudonetwork. Thus, the calculation of the finite extensibility component according to (1) is done in a two-chain and not, as usually, in a single-chain approach. The constraining tubes are assumed to give rise to an increased orientation of the chain segments. From (5) and (6), we then find

$$n = n(\lambda) = \frac{A\hat{\rho}_p RT}{G(\lambda)M_s} \tag{8}$$

$\hat{\rho}_p$ is the mass density of the elastically effective network, which is taken to equal the mass density of the polymer ρ_p in a first approximation, where network defects are neglected. $M_s = M_m \cdot C_\infty$ is the molar mass of a statistical segment, i.e., the monomer molar mass M_m multiplied by the characteristic ratio C_∞ of the polymer.‡

By combining eqs. (1) and (8), we find

$$n = \frac{A\hat{\rho}_p RT}{\sigma_{\text{red}} M_s}\left\{1 + \frac{3}{25n}\left(3\lambda^2 + \frac{4}{\lambda}\right) + \cdots\right\} \tag{9}$$

If the series expansion (1) is taken up to fourth order in n, this is an equation of fifth order in n, which can be solved explicitly by elementary numerical calculations for every stress–strain measurement point. As a result, the finite extensibility component can be separated from the reduced stress and the Gaussian contribution to the reduced stress $G(\lambda)$ as well as G_1 and G_2 can be calculated in a first approximation.

In view of obtaining more exact values for the finite extensibility component of the reduced stress, two of the above assumptions have to be modified. On the one hand, the value of the structure factor A, which was taken within the framework of free fluctuating cross-links, has to be calculated more exactly. On the other hand, the mass density of the polymer used in eq. (8) has to be replaced by the mass density of the elastically effective network, i.e., the dangling chain ends have to be substracted. This is done later, by using Langley's trapping factor. Here, we first focus on the structure factor A, which is now coupled to the real amount of fluctuations of the cross-links.

2.2. Calculation of the Structure Factor

As already remarked above, the tube model does not necessarily predict a free fluctuating phantom network in the infinite-strain limit. This is only found for highly swollen networks, where the constraint modulus vanishes totally. In dry rubber networks, the restrictions on junction fluctuations resulting from the surrounding chains do not disappear asymptotically in the infinite-strain limit. The tube model explains the asymptotic release of the constraint modulus by a special deformation behavior of the tubes and not by a release of the constraints on the junctions, as assumed in the theory of restricted junction fluctuations. A calculation of the structure factor within the framework of the tube model was made by Kästner.[16] It takes into account that the constraints acting on a cross-link are gen-

† This mean-field picture with a strain-dependent elastically effective strand density is mathematically equivalent to a tube model with strain-dependent tube diameters, where the components in direction of the principal axis of the deformation tensor change as

$$d_i = d_0\lambda_i^{1/2}; \qquad i = 1, 2, 3 \tag{7}$$

d_0 is the diameter of the tube in the undeformed state and d_i is the diameter in direction i of the principal axis system in the deformed state. This model was derived self-consistently by Heinrich et al.[6,19,20] for moderately but almost completely cross-linked networks, where the degree of coil interpenetration is high and the constraining tubes are governed by a large number of chains.

‡ The definition of C_∞ used here differs from the one found in the polymer handbook and other literature.[29–31] Here, C_∞ is related to the length of a monomer unit and not to the average bond length of the chain backbone.

erally stronger than those acting on chain segments distant from the cross-links:

$$A = 1 - \frac{2}{f}\left\{1 - \frac{2}{\sqrt{\pi}}\frac{K \cdot e^{-K^2}}{\operatorname{erf} K}\right\} \tag{10}$$

where

$$K = \sqrt{\frac{3f}{2}}\frac{r_0}{R_0} \tag{11}$$

r_0 is the tube radius in the undeformed state and R_0 is the mean end-to-end distance of the elastically effective strands. Thus, A depends not alone on the functionality f of the cross-links, but it is influenced as well by the ratio between r_0 and R_0. This can also be expressed by the ratio between G_1 and G_2, because "Kuhn's square root law," respectively, the tube model, implies[6]

$$G_1 = A\nu_1 RT = \frac{A\hat{\rho}_p l^2 RT}{R_0^2 M_s} \tag{12}$$

$$G_2 = \frac{\beta^2 \hat{\rho}_p l^2 RT}{4\sqrt{6} M_s r_0^2} \tag{13}$$

ν_1 is the density of elastically effective strands; r_0, the tube radius, which determines the mean fluctuation space of the chain segments; and l, the Kuhn's step length of a statistical segment. The parameter K can now be rewritten as

$$K = \sqrt{\frac{3f\beta^2}{8\sqrt{6}A}\frac{G_1}{G_2}} \tag{14}$$

By taking the experimental values of G_1 and G_2 from the first approximation and repeating the above-described numerical procedure for calculating the finite extensibility component of the reduced stress with the improved values of A, a second approximation for G_1, G_2, and A can be found iteratively. In view of obtaining a third approximation, we will now take into account the elastically ineffective network strands, i.e., the dangling chain ends that are connected very close to the trapping of interchain entanglements. The elastically ineffective closed loops are not regarded at this stage (compare Fig. 2).

2.3. Network Defects and Trapped Entanglements

Most of the polymer networks used in practice contain a more or less considerable amount of network defects. These result mainly from chain-scission effects during the cross-linking procedure or in the case of end-group cross-linking from incomplete cross-linking reactions. Both of these effects are connected very close to the fraction T_e of interchain entanglements that are trapped during the cross-linking procedure. Thus, they are conveniently described with the help of Langley's trapping factor T_e, which can be used for counting the elastically effective strands of a network.[32-34] Two different methods of counting effective strands are found in the literature.[34-36] We will apply them by restricting ourselves to the case $f = 4$ of tetrafunctional cross-links.

One obvious method of counting effective strands was given by Scanland.[35] His method counts two effective strands per cross-link that is connected to the gel by all four paths, plus 1.5 effective strands per cross-link that is connected by three paths. It results in the following relation between the mass density of the elastically effective network $\hat{\rho}_p$ and the mass density of the whole network ρ_p:

$$\hat{\rho}_p = \left(\frac{3}{2}\sqrt{T_e}w_g - \frac{T_e}{2}\right)\rho_p \tag{15}$$

w_g is the gel fraction of the network, which has a value very close to one in highly extendable networks. It equals the probability that a randomly chosen segment of the network is connected to the gel by at least one path. $\sqrt{T_e}$ is the probability that a randomly chosen segment is connected to the gel by both paths.

A second method of counting effective strands was introduced by Flory.[36] He counted two effective strands per cross-link that is connected to the gel by all four paths, but only one effective strand per cross-link that is connected by three paths. This method is related to the cycle rank concept of Flory and frequently used for calculating the relation between the elastically effective strand density ν_c due to the cross-links and the corresponding cross-linking density μ_c:

$$\nu_c = 2\sqrt{T_e}w_g\mu_c \tag{16}$$

The effect of network defects on the structure factor A, which results from a reduction of the functionality of some cross-links, is exactly canceled by using Flory's method of counting effective strands. This means that the maximum value of the functionality $f = 4$ can be used in calculations, if Flory's method, i.e., eq. (16), is applied. An alternative possibility is the use of Scanland's method of counting effective strands,[35] but, then, a mean functionality

has to be used upon calculation of A. Instead of eq. (16), we then find

$$\nu_c = (3\sqrt{T_e}w_g - T_e)\mu_c \qquad (16')$$

In both cases, the elastically effective strand density ν_c is coupled to a corresponding infinite-strain modulus G_c via the structure factor A, which has to be calculated by using the maximum value or a mean value of the functionality, respectively:

$$G_c = A\nu_c RT \qquad (17)$$

In general, the modulus G_c is identified by the C_1 term of the Mooney–Rivlin equation, but here we assume, as already discussed above, that an additional influence of trapped entanglements governs the infinite-strain modulus G_1:

$$G_1 = G_c + G_e T_e \qquad (18)$$

This assumption is confirmed in the experimental part of this paper (compare Fig. 6). The modulus G_e due to entanglements has the same structure (17) as does G_c; however, the structure factor A is not the same because the fluctuation range of entanglements differs from that of cross-links. Therefore, an experimental determination of the trapping factor T_e from the structure of the elastic modulus G_1 as given by eq. (18) is not possible as long as the structure factor of the modulus G_e remains unknown.

The significance of T_e for a characterization of networks covered with defects becomes obvious in view of eqs. (15), (16), and (16'): An experimental determination of cross-linking densities as well as dangling chain ends from stress–strain measurement data requires knowledge of the trapping factor. The classical experimental procedure to find it consists of a measurement of the molecular weight before cross-linking and the extractable sol fraction in the network, from which the value of the trapping factor can be calculated.[33,34] However, a determination of the sol fraction in highly defective networks is complicated by the fact that the sol particles are difficult to extract, because they can be branched. In the following part of this paper, we will introduce an alternative procedure, which determines the trapping factor from the structure of the constraint modulus.

2.4. Determination of the Trapping Factor

The constraint modulus G_2 as calculated from the tube model (13) depends on the mean fluctuation length of the chain segments, which is called the tube diameter. In view of finding the trapping factor, this quantity is coupled to the mean spacing of the topological constraint centers, which are built by the chemical cross-links as well as by the entanglements. For simplification, we will first demonstrate how this is done in the melt case, where chemical cross-links and chain-scission effects are absent. The plateau modulus G_N^0 of the melt then reads

$$G_N^0 = \tfrac{8}{5}\mu_e RT \qquad (19)$$

and

$$\mu_e = \frac{\rho_p l^2}{2M_s(\xi r_0^{\text{melt}})^2} \qquad (20)$$

μ_e is the density of entanglements in the melt and ξ is a proportionality constant between the tube radius in the melt r_0^{melt} and the mean spacing of entanglements along a single chain:

$$\xi = \frac{\sqrt{N_e}\,l}{r_0^{\text{melt}}} \qquad (21)$$

N_e is the mean number of statistical segments between entanglements. In some applications, ξ is taken to be one[6]; however, we will see below that this is not consistent in our model and ξ has a value around two.

In the next step, we will now generalize these considerations to the case of networks covered with defects. We assume that the defects are caused by main-chain scission, which also frees entanglements. Even at relatively low scission levels, many entanglements are not trapped because they are freed by producing a free chain end from one of the four strands. The portion of entanglements that are freed and not trapped cannot contribute to the moduli G_1 and G_2 if the characteristic deformation time in stress–strain measurements is smaller than the relaxation time determined by the size of the free ends. This means that at relatively high cross-linking densities, where the trapping factor has reached a limiting value $T_{e,\max}$ and no more trapping takes place, the density of topological constraint centers μ_{ce} is given by (compare Fig. 1)

$$\mu_{ce} = \mu_c + \mu_e T_{e,\max} = \frac{\hat{\rho}_p l^2}{2M_s(\xi r_0)^2} \qquad (22)$$

This expression is built in analogy to eq. (20), where the tube radius r_0 in the network, as given by the

constraint modulus G_2, is used. The dependency on the mass density $\hat{\rho}_p$ of the elastically effective network and not on the mass density ρ_p of the whole network reflects the fact that entanglements of the dangling free chain ends give no contribution to the constraint modulus. The parameter ξ is assumed to be independent of cross-linking density. In the network case, it determines the ratio between the mean spacing of the constraint centers along a single chain and the tube radius:

$$\xi = \frac{\sqrt{N_{ce}}\,l}{r_0} \qquad (21')$$

N_{ce} is the mean number of statistical segments between the constraining centers. By using eq. (22) and combining it with eqs. (13), (16), (17), and (19), we can now find a relation between the moduli G_c, G_2, and G_N^0:

$$G_c = \frac{4Aw_g\sqrt{6T_{e,\max}}}{(\xi\beta)^2}\,G_2 - \frac{5Aw_g}{4}\,G_N^0 T_{e,\max}^{3/2} \qquad (23)$$

As the limiting value of the trapping factor is independent of cross-linking densities, this relation allows the determination of $T_{e,\max}$ from the axis intersection of a plot of G_c against G_2. For the structure factor A, which slightly depends on cross-linking densities, a mean value has to be used. The gel fraction w_g can taken to be equal to one, because in highly extendable networks, it always has a value very close to one.

The limiting value of the trapping factor $T_{e,\max}$ depends on the scission level only and not on the initial molecular weight distribution. This is because there are many more scission-produced chain ends than original ends if scission occurs. By assuming the relative scission probability p/q to be constant, we find[33]

$$T_{e,\max} = \frac{1}{16}\left[3 - \left(1 + 4\,\frac{p}{q}\right)^{1/2}\right]^4 \qquad (24)$$

p is the probability that a randomly chosen chain segment suffers scission and q is the corresponding probability that it is cross-linked during the curing process.

3. RESULTS

Natural rubber samples (SMR CV 50) were cured with two different cross-linking systems at 155°C up to 90% of the maximal torque found in vulcameter measurements. In one case, peroxid (DCP) was employed, and in the other case, thiuram (TMTD) together with the same amount of ZnO was used. The amount of cross-linking agent was varied systematically. Stress–strain measurements were executed at the cured samples in uniaxial extension (Universalprüfmaschine Zwick 1445). To avoid stress-induced crystallization, the measurements were performed in a temper box at 100°C. The deformation velocity was chosen to be small (10 mm/min) in order to evade dynamical contributions to the modulus.

Figure 3 shows a typical example of measured reduced stress curves plotted against the inverse deformation ratio. In addition, the numerically calculated Gaussian contribution $G(\lambda)$ of the reduced stress according to eq. (1) combined with eqs. (8), (10), and (15) is shown. Every point of the Gaussian contribution was calculated iteratively by solving eq. (9) up to fifth order in n. It is important to note that this order of the equation should not be reduced, because the series expansion (1) converges very slowly for large values of λ or small n. The characteristic ratio was taken to be $C_\infty = 1.9$ i.e., the mol mass of the statistical segments results as $M_s = M_m \cdot C_\infty = 129$ g/mol. This number represents the mean of several values given by different references.[6,29,30] The mass density of the samples was measured as $\rho_p = 900 \pm 5$ kg/m^3 and the functionality of the cross-links was taken to be $f = 4$. The trapping factor T_e was taken from the plot in Figure 8.

The regression line inserted in Figure 3 determines the moduli G_1 and G_2. It is seen that the Gaussian modulus $G(\lambda)$, as calculated according to eq. (1), fulfills eq. (3) even up to large extensions where the "upturn" of the reduced stress appears. The observed deviations from the postulated behavior (3) at very large extensions can be explained by a bursting of single short chains, which result from inhomogeneities in the network. The deviations at small extensions are possibly due to energy-elastical contributions to the modulus, resulting from intermolecular interactions in the domain of the cross-linking points. However, these deviations can as well be attributed to experimental difficulties to make an unambiguous definition of the unstrained length l_0 of the sample, which is associated with the lack of perfect reversibility of the rubber. Any small error in l_0 has an exaggerated effect on the measured zero-strain limit. This means that the experimental method of uniaxial extension is not appropriate for the determination of the reduced stress in the zero-

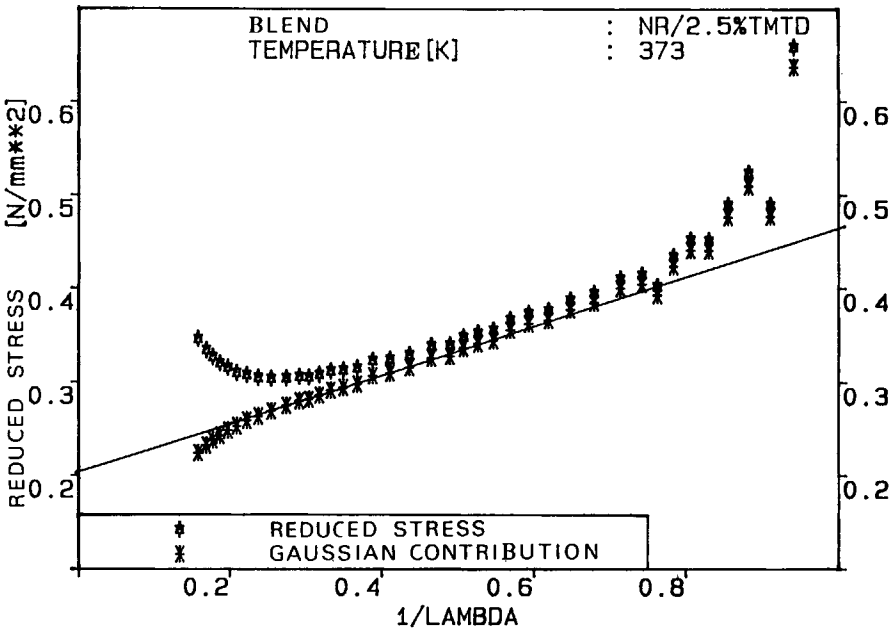

Figure 3 Typical example of a Mooney–Rivlin plot for the reduced stress. For every measurement point, in addition, the numerically calculated Gaussian contribution is shown.

strain limit if the zero of strain cannot be associated quite exactly with the zero of stress.

Figures 4 and 5 show the reduced stress and the calculated Gaussian contribution for four different degrees of cross-linking with TMTD and DCP, respectively. The influence of the strain and the degree of cross-linking on the orientation of the chains, as stated by eq. (1), becomes obvious: The degree of cross-linking or, equally well, the number of statistical segments between cross-linking points n determines the "position of the upturn" according to the equation $\lambda_{max} = \sqrt{n}$, where (1) approaches infinity. In addition, n determines the amount of deviation between the reduced stress and the Gaussian contribution. This finite extensibility component of the reduced stress increases with rising degree of cross-linking. It results in a systematic decrease of the infinite-strain limit G_1 compared to the predictions of the Mooney–Rivlin procedure that assumes a purely Gaussian network model. This was already pointed out by Mullins and Morris.[37,38] The constraining part G_2, i.e., the slope of the regression lines in Figures 4 and 5, is generally more distinct than in the Gaussian theory, where the finite extensibility of the polymer chains is not taken into account.

Figures 6 and 7 show the infinite-strain limits G_1 of the TMTD and DCP networks as a function of curing-agent concentration. It becomes obvious that G_1 is influenced by chemical cross-linkings as well as by trapped entanglements. The experimental results confirm the assumed decomposition (18) of G_1.

The trapping factor T_e increases with rising TMTD or DCP concentration and reaches a limiting value $T_{e,max}$ at about 100 mol/m^3 TMTD and 35 mol/m^3 DCP, respectively. At this point, all entanglements that are not freed by main-chain scission are trapped by the chemical cross-links and no more trapping takes place. (If no scission occurs, we have $T_{e,max} = 1$.) The dotted lines represent an extrapolation of the limiting value $T_{e,max}$ to zero cross-linking densities. The intersections with the axis determine the limiting contributions $G_e T_{e,max}$ of the entanglements to the modulus G_1 according to eq. (18). Compared to the chemical cross-links, these contributions are relatively small. However, this does not mean that the limiting number of trapped entanglements is small compared to the cross-links. This is because a trapped entanglement lowers the degree of freedom of the network less than that of a chemical cross-link, i.e., the fluctuation range of trapped entanglements is larger and, thus, the structure factor is smaller than the corresponding one of chemical cross-links. This results in a smaller contribution of a trapped entanglement to the elastic modulus G_1 compared to a chemical cross-link. An experimental determination of the limiting values $T_{e,max}$ from the plots in Figures 6 and 7 is complicated by this fact.

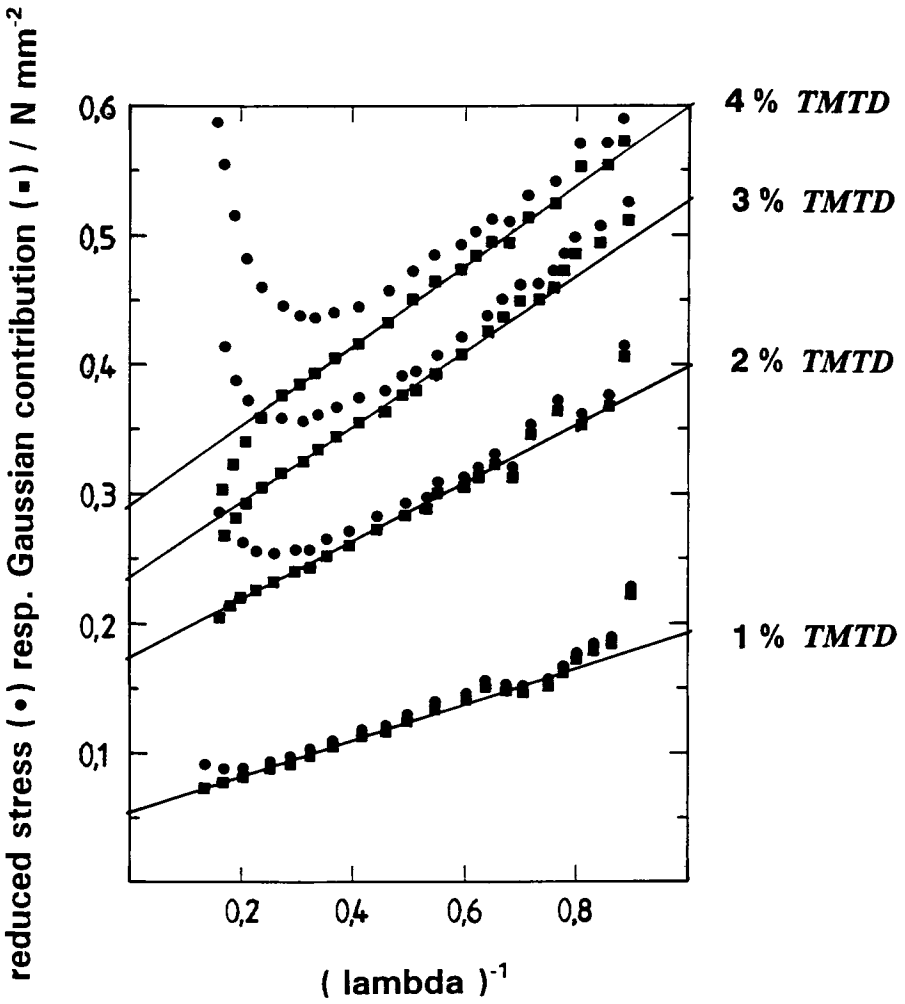

Figure 4 Mooney–Rivlin plots of the reduced stress (●) at $T = 100°C$ and the calculated Gaussian contribution (■) for natural rubber networks, cured with 1, 2, 3, and 4 wt % thiuram (TMTD).

An easier way of evaluating the limiting values of the trapping factor is found by using the plot in Figure 8, where the constraint moduli G_2 of both the TMTD and DCP networks are plotted against the elastic moduli G_c due to the chemical cross-links, i.e., the moduli G_1 shown in Figures 6 and 7 minus the axis intersections [compare eq. (18)]. Not all measured values are indicated in Figure 8, but only those of higher cross-linking densities where the trapping factor has reached its limiting value $T_{e,\max}$. The regression lines inserted correspond to the predictions of eq. (23). From the slopes and the axis intersections of these lines, the limiting values of the trapping factor $T_{e,\max}$ of both network types as well as the proportionality constant ξ defined in (21) can be evaluated. The results are shown in Table I. For the structure factors, mean values of $\bar{A} = 0.81$ and 0.76 have been used (compare Fig. 10), whereas the gel fraction w_g was taken to be equal to one. The plateau modulus of the natural rubber melt was found from dynamical measurements to be $G_N^0 = 0.5$ N mm^{-2}.

The two limiting values of the trapping factor, which are independent of cross-linking density, allow the calculation of the limiting fractions of the elastically effective network chains and the relative chain-scission probabilities by using eqs. (15) and (24). These results are independent of cross-linking density as well. They are shown in Table I together with the cross-linking efficiencies, i.e., the number of cross-links per TMTD and DCP molecules. These values are found from the slopes of the dotted lines in Figures 6 and 7 together with eqs. (16) and (17). The relatively small efficiency in the TMTD cross-

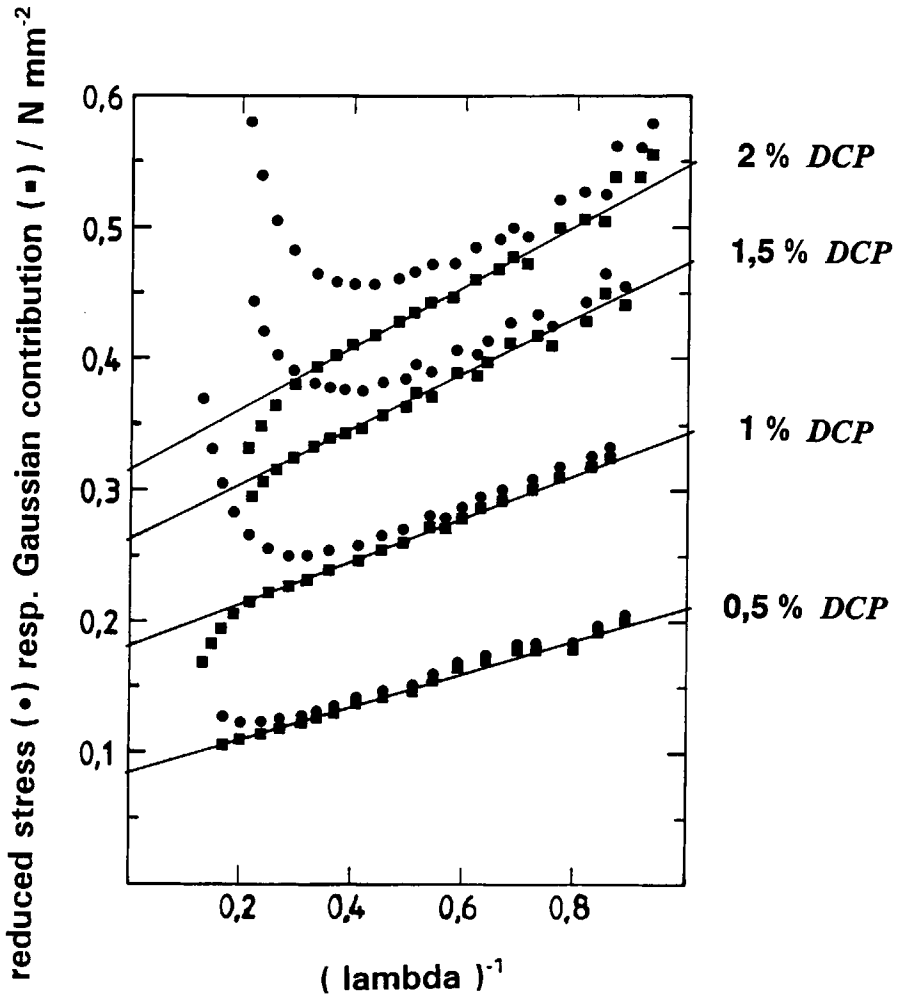

Figure 5 Mooney–Rivlin plots of the reduced stress (●) at $T = 100°C$ and the calculated Gaussian contribution (■) for natural rubber networks, cured with 0.5, 1, 1.5, and 2 wt % peroxid (DCP).

linking procedure indicates that only a small part of the TMTD radicals creates cross-links. Most is wasted in a subsidiary reaction. For the DCP cross-linking procedure, this is not the case; however, 21% of the DCP radicals led to main-chain scission.

Figure 9 shows the infinite-strain moduli G_1 as a function of the calculated cross-linking densities for both cross-linking systems. The regression lines inserted correspond to the limiting numbers of trapped entanglements. The slope of the lines is governed mainly by the root of the limiting value of the trapping factor as given by eq. (16). It is seen that the highly defective DCP networks have generally smaller elastic equilibrium moduli than that of the nearly perfect TMTD networks without defects if the number of cross-links is taken to be the same in both cases. This is because the chain ends do not contribute to the equilibrium modulus and, thus, the number of elastically effective strands, which determines the modulus G_1 according to eq. (12), is reduced in defective networks. An additional but smaller effect results from the differences in the structure factor A. The values of A as calculated from eqs. (10) and (14) are plotted in Figure 10. They all lie in between the free fluctuation limit $A = \frac{1}{2}$ and the affine, nonfluctuating limit $A = 1$.

4. CONCLUSIONS

The experimental results show that the amount of main-chain scission during the cross-linking procedure, which determines the dangling free chain ends and trapped entanglements, can be evaluated

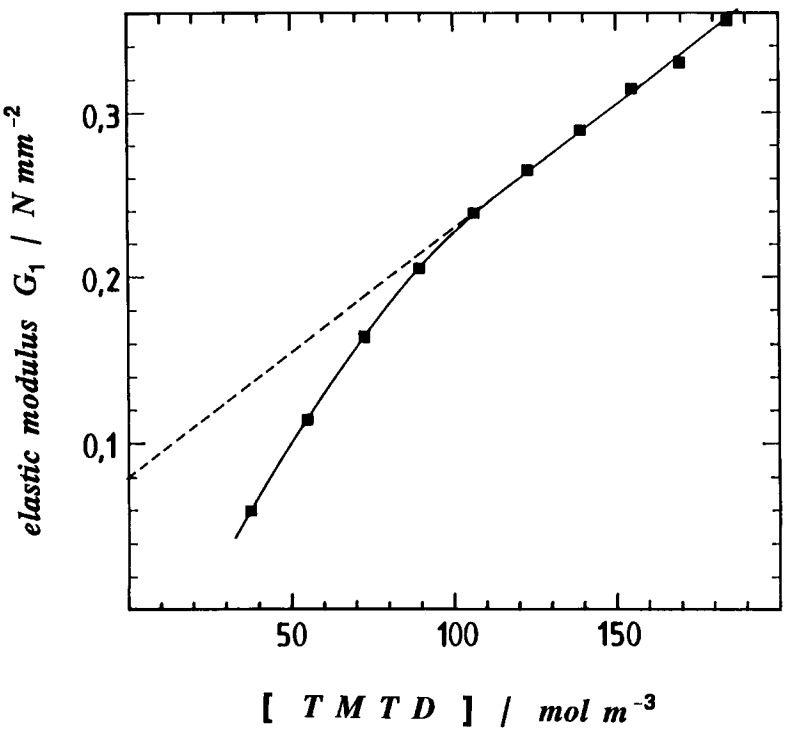

Figure 6 Plot of the elastic modulus G_1 vs. the TMTD concentration. The extrapolation at vanishing TMTD concentration (dotted line) determines the limiting contribution of trapped entanglements.

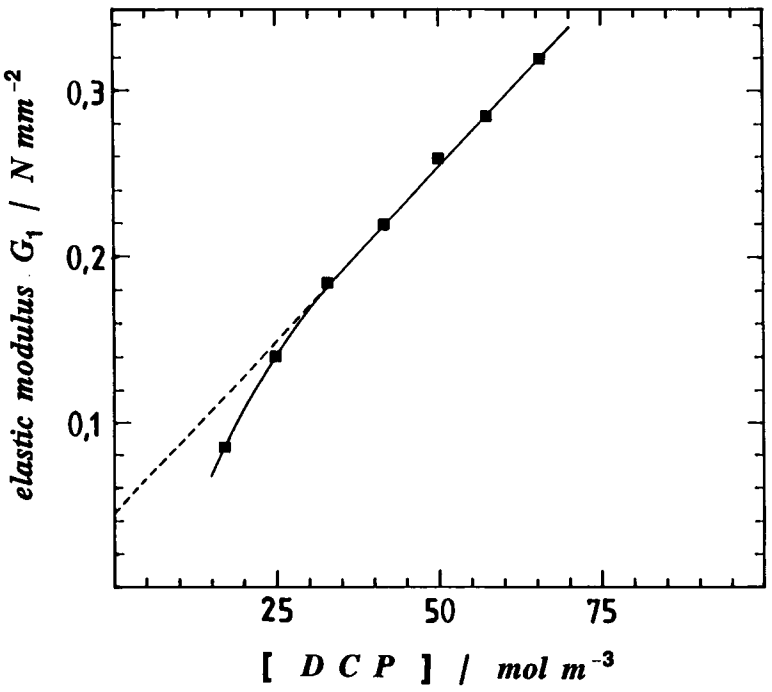

Figure 7 Plot of the elastic modulus G_1 vs. the DCP concentration. The extrapolation at vanishing DCP concentration (dotted line) determines the limiting contribution of trapped entanglements.

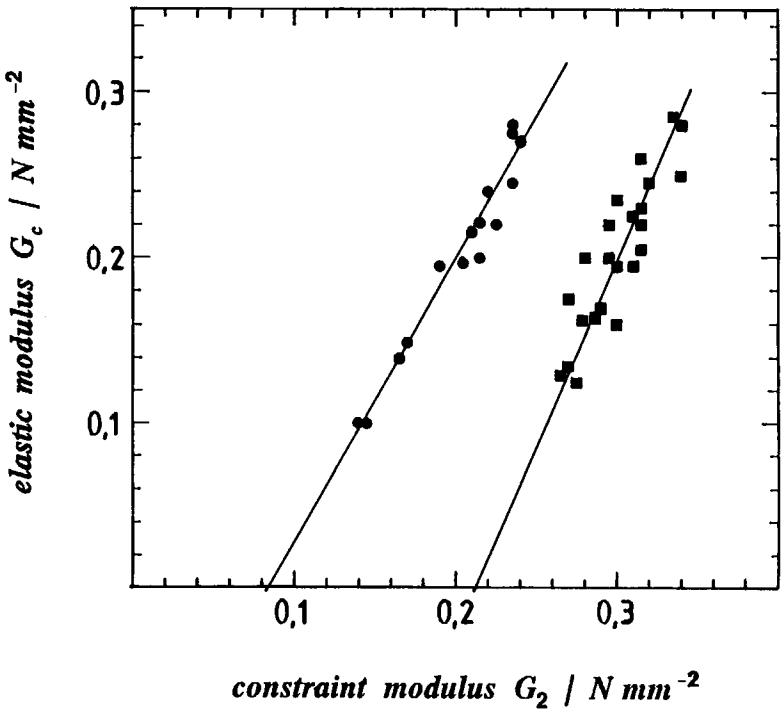

Figure 8 Plot of the moduli G_c due to chemical cross-links vs. the constraint moduli G_2. The regression lines inserted determine the limiting values of the trapping factor $T_{e,max}$ according to eq. (23). (■) TMTD networks; (●) DCP networks.

from the stress–strain behavior of the networks at large extensions. A necessary requirement is the consideration of the finite extensibility component of the reduced stress. Otherwise, the determination of the limiting value of the trapping factor according to the plot in Figure 8 results in an inconsistency, because the value for the TMTD networks becomes larger than one. The calculated values that are smaller, but quite close to one, confirm the proposed model. If TMTD is used in the cross-linking procedure, nearly all (96%) entanglements are trapped and only 1% dangling free chain ends result in the limit of high cross-linking densities. These are possibly induced by thermal scission, because the thermal stability of natural rubber is not good. However, if the cross-linking procedure is performed with DCP, only 45% of the entanglements in the melt are trapped and 22% dangling free chain ends result in the limit of high cross-linking densities. Obviously, the corresponding relatively high chain-scission probability $p/q = 0.21$ is induced by reactions of the cross-linking agent itself. The causal connections of these reactions cannot be clarified in the framework of this paper. To find them, additional comparing examinations using polymers with different structures have to be done.

Instead, we will focus on another question of interest, which concerns the tensile strength properties of the two types of networks in the soft rubber range. It is found that the TMTD networks have generally better tensil strength properties than do the DCP networks. An obvious conclusion is the connection

Table I Characteristic Network Parameters That Are Independent of Cross-linking Densities

	$T_{e,max}$	ξ	$\hat{\rho}_p/\rho_p$	p/q	$\frac{\mu_c}{[TMTD/DCP]}$
NR/TMTD	0.96	1.86	0.99	0.01	0.31
NR/DCP	0.45	1.71	0.78	0.21	1.33

$T_{e,max}$: limiting value of the trapping factor; $\hat{\rho}_p/\rho_p$: limiting fraction of elastically effective network chains; p/q: relative chain-scission probability; μ_c/[TMTD/DCP]: cross-linking efficiency.

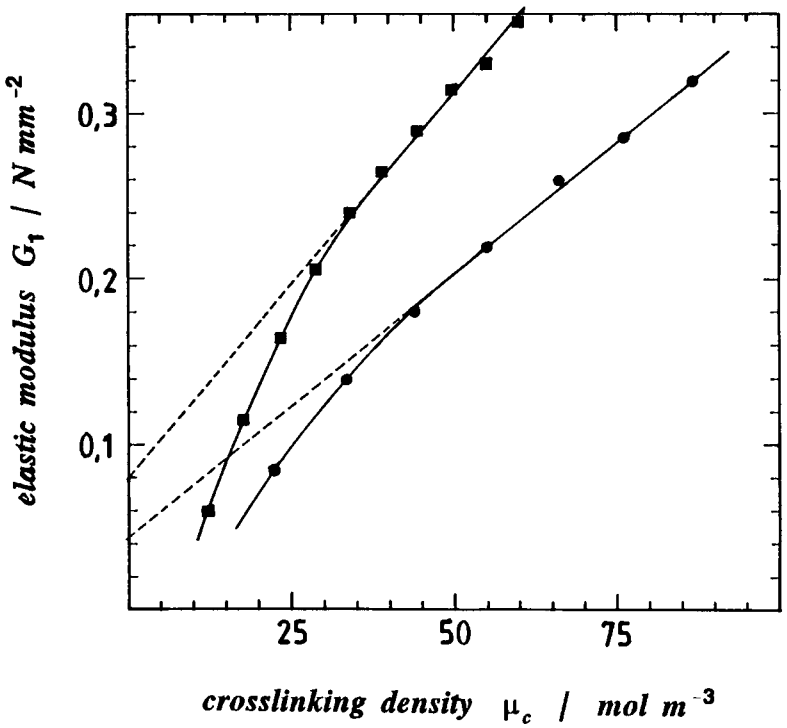

Figure 9 Plot of the elastic moduli G_1 vs. the calculated cross-linking density. The slope of the regression lines is governed by the different amounts of elastically effective strands. (■) TMTD networks; (●) DCP networks.

of this fact with the different amounts of network defects: On the one hand, the dangling free chain ends can be imagined to reduce the tensile strength, because they do not contribute to the elastic modulus and just result in a "dilution" of the network. However, this effect is small and we adopt the view that the tensile strength properties in the soft rubber range are governed mainly by the number of trapped

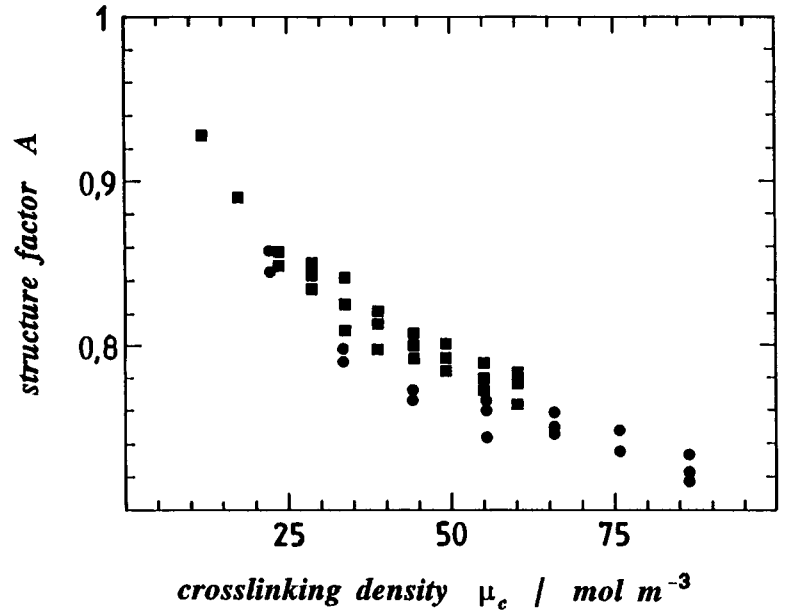

Figure 10 Plot of the calculated structure factors A vs. the cross-linking density. (■) TMTD networks; (●) DCP networks.

entanglements directly. This follows from the assumption that the tensile strength depends on the width of distribution of the chain lengths, i.e., the degree of homogeneity in the network.

Concerning this line of reasoning, good tensile strength properties require a uniform distribution of stress on all network chains or, equally well, a smoothening of stress peaks in the network. Trapped entanglements induce such a smoothening effect, because they are allowed to slide across each other up to an equilibrium position where all entangled chains are stressed uniformly. This effect governs the tensile strength properties of rubber networks as long as the number of trapped entanglements is larger or of the same order as the number of cross-links. Beyond this range, the tensile strength properties are determined by the inhomogeneities of the strands due to the chemical cross-links alone, because the probability that two cross-links are separated by a homogenizing entanglement decreases rapidly.

This means that the tensile strength of rubber networks passes through a maximum in the soft rubber range, which is indeed found in experimental results. The position as well as the value of the maximum is determined by the number of trapped entanglements.

From statistical arguments, it is clear that the position of the maximum should be defined independently of the kind of network by a critical ratio between the strand density ν_c and the density of trapped entanglements $\mu_e \cdot T_{e,\max}$. The experimental results found on the TMTD and DCP networks suggest this ratio to have a value around one. A more exact determination of the critical ratio requires additional examinations of other networks.

The author wishes to thank Dr. R. Badura for the generous support of this work and Dr. G. Heinrich for several useful hints and inspiring discussions. Thanks are due also to Mr. Y. Yongwei for the programming of the numerical procedure and Mr. A. Bischoff for the preparation of the networks.

REFERENCES

1. L. R. G. Treloar, *The Physics of Rubber Elasticity,* 3rd ed., Clarendon Press, Oxford, 1975.
2. P. J. Flory, *Principles of Polymer Chemistry,* Cornell University, Ithaca, NY, 1953.
3. K. Dusek and W. Prins, *Adv. Polym. Sci.*, **6,** 1 (1969).
4. W. Burchard, *Ber. Bunsenges. Phys. Chem.*, **89,** 1154 (1985).
5. G. Heinrich, E. Straube, and G. Helmis, *Acta Polym.*, **31,** 275 (1980).
6. G. Heinrich, E. Straube, and G. Helmis, *Adv. Polym. Sci.*, **85,** 33 (1988).
7. S. F. Edwards and T. A. Vilgis, *Rep. Prog. Phys.*, **51,** 243 (1988).
8. W. Kuhn, *Kolloid Z.*, **68,** 2 (1934); **76,** 258 (1936); **87,** 3 (1939).
9. E. Guth and H. Mark, *Monatsh. Chem.*, **65,** 93 (1934).
10. P. J. Flory, *J. Chem. Phys.*, **66,** 5720 (1977).
11. P. J. Flory, *Polymer,* **20,** 1317 (1979).
12. P. J. Flory and B. Erman, *Macromolecules,* **15,** 800 (1982).
13. P. J. Flory, *Polym. J.*, **17,** 1 (1985).
14. S. Kästner, *Faserf. Textilt./Z. Polymerforsch.*, **27,** 1 (1976).
15. S. Kästner, *Acta Polym.*, **31,** 444 (1980).
16. S. Kästner, *Colloid Polym. Sci.*, **259,** 499, 508 (1981).
17. S. Kästner, *Polymer,* **20,** 1327 (1979).
18. W. Gronski, D. Emeis, A. Brüderlin, M. Maldaner Jacobi, R. Stadler, and K. Eisenbach, *Br. Polym. J.*, **17,** 103 (1985).
19. G. Heinrich and E. Straube, *Polym. Bull.*, **17,** 247 (1987).
20. G. Heinrich and E. Straube, *Acta Polym.*, **35,** 115 (1984).
21. G. Heinrich, E. Straube, and G. Helmis, *Z. Phys. Chem. (Leipzig),* **258,** 361 (1977).
22. G. Heinrich, E. Straube, and G. Helmis, *Z. Phys. Chem. (Leipzig),* **260,** 737 (1979).
23. G. Heinrich, *Plaste Kautsch,* **29,** 437 (1982).
24. N. W. Tschoegl, in *Abstracts 9th Europhys. Conference, Macromol. Phys.*, Jablonna, Poland, 1979.
25. W. Gronski, Lecture presented at a Rubber Colloquium of the Deutsches Institut für Kautschuktechnologie e. V. (DIK) (German Rubber Institute), Hannover, Germany, March, 1991.
26. T. A. Vilgis, *Kautsch. Gummi Kunstst.*, **42,** 475 (1989).
27. W. Kuhn and F. Grün, *Kolloid Z.*, **101,** 248 (1942).
28. W. Kuhn and H. Kuhn, *Helv. chim. Acta,* **29,** 1095 (1946).
29. J. Bandrup and E. H. Immergut, Eds., *Polymer Handbook,* 2nd ed., Wiley-Interscience, New York, 1975.
30. S. M. Aharoni, *Macromolecules,* **16,** 1722 (1983).
31. J. F. Flory, *Statistical Mechanics of Chain Molecules,* Wiley-Interscience, New York, 1969.
32. M. Inokuti, *J. Chem. Phys.*, **38,** 2999 (1963).
33. N. R. Langley, *Macromolecules,* **1,** 348 (1968).
34. N. R. Langley and K. E. Polmanteer, *J. Polym. Sci. Polym. Phys.*, **12,** 1023 (1974).
35. J. Scanlan, *J. Polym. Sci.*, **43,** 501 (1960).
36. P. J. Flory, *Chem. Rev.*, **35,** 51 (1944).
37. L. Mullins, *J. Appl. Polym. Sci.*, **2,** 257 (1959).
38. M. C. Morris, *J. Appl. Polym. Sci.*, **8,** 545 (1964).

Received January 6, 1992
Accepted June 30, 1992